

Effective Majorana mass and neutrinoless double beta decay

Giovanni Benato^a

Physik Institut der Universität Zürich, Zurich, Switzerland

Received: 6 October 2015 / Accepted: 13 November 2015 / Published online: 28 November 2015
© The Author(s) 2015. This article is published with open access at Springerlink.com

Abstract The probability distribution for the effective Majorana mass as a function of the lightest neutrino mass in the standard three neutrino scheme is computed via a random sampling from the distributions of the involved mixing angles and squared mass differences. A flat distribution in the $[0, 2\pi]$ range for the Majorana phases is assumed, and the dependence of small values of the effective mass on the Majorana phases is highlighted. The study is then extended with the addition of the cosmological bound on the sum of the neutrino masses. Finally, the prospects for $0\nu\beta\beta$ decay search with ^{76}Ge , ^{130}Te and ^{136}Xe are discussed, as well as those for the measurement of the electron neutrino mass.

1 Introduction

Neutrinoless double beta decay ($0\nu\beta\beta$) is a topic of major interest for the present and near future of neutrino physics [1]. Its detection would prove the violation of total lepton number conservation and provide information on the absolute neutrino mass scale. In the following the assumption is made that the standard light neutrino exchange is the dominant contribution. The parameter of interest in $0\nu\beta\beta$ decay is the so-called effective Majorana mass, $|m_{\beta\beta}|$, which depends on the three neutrino mass eigenstates, on two of the PMNS mixing angles, and on two Majorana phases [1]. Currently, a good knowledge of the two squared mass differences and of the mixing angles is available thanks to accelerator and reactor experiments [2]. Moreover, some bound on the sum of neutrino masses is available from cosmological observations [3,4]. On the contrary, assuming that neutrinos are Majorana particles, no information is available on the Majorana phases.

Typically, the allowed range for $|m_{\beta\beta}|$ as a function of the lightest neutrino mass is calculated via an error propagation on the involved mixing angles and squared mass differences.

The computation is performed for the values of the Majorana phases yielding the largest and smallest $|m_{\beta\beta}|$, and the obtained regions are merged. In this way, no clear information is given about the most probable value of $|m_{\beta\beta}|$ within the allowed region. Recently, the cosmological limit has been introduced, too [5].

In the present paper, an alternative approach for the extraction of the effective mass allowed regions is exploited. Instead of presenting only e.g. 3σ coverage regions for the $|m_{\beta\beta}|$, a probability distribution is given, which can be valuable for the design of experiments. This is extracted via random sampling on the probability distributions of the measured parameters and on a flat distribution for the Majorana phases.

After a short formulation of the problem in Sect. 2, the probability distribution for $|m_{\beta\beta}|$ as a function of the lightest neutrino mass is reported in Sect. 3. The $|m_{\beta\beta}|$ dependence on the values of the Majorana phases is highlighted, and the case of vanishing $|m_{\beta\beta}|$ is discussed. In Sect. 4, the cosmological bound on the sum of the neutrino masses is inserted in the calculation and its influence in the distributions is described. The perspectives for $0\nu\beta\beta$ decay search given this study of $|m_{\beta\beta}|$ and the present knowledge of the nuclear matrix elements are presented in Sect. 5. Additionally, the probability distribution for $|m_{\beta\beta}|$ as a function of the electron neutrino mass is given in Sect. 6, and the physics reach of beta spectrum end point measurements is discussed.

The aim of this paper is to prove the possibility of using the information on the sum of neutrino masses provided by the cosmological measurements, and to demonstrate the dependence of the effective mass on the assumption made for the Majorana phases. The comparison of such different assumptions can provide a deeper understanding of the current status and the perspective of $0\nu\beta\beta$ decay search.

2 Effective Majorana mass

The parameter of interest in the $0\nu\beta\beta$ decay search is $|m_{\beta\beta}|$. It is a combination of the neutrino mass eigenstates and the

^a e-mail: gbenato@physik.uzh.ch

neutrino mixing matrix terms. Under the hypothesis that only the known three light neutrinos participate in the process, the effective mass is given by

$$|m_{\beta\beta}| = \left| \sum_{i=1}^3 U_{ei}^2 m_i \right| \quad (1)$$

where U is the PMNS mixing matrix [1], with two additional Majorana phases. The expansion of Eq. 1 yields

$$|m_{\beta\beta}| = |c_{12}^2 c_{13}^2 m_1 + s_{12}^2 c_{13}^2 m_2 e^{i\alpha} + s_{13}^2 m_3 e^{i\beta}| \quad (2)$$

where the CP-violating phase present in the PMNS matrix is hidden in the Majorana phases α and β . In this formulation, the symbols c_{jk} (s_{jk}) stay for $\cos \theta_{jk}$ ($\sin \theta_{jk}$). Expanding Eq. 2 and following the definition of absolute value for complex numbers:

$$|m_{\beta\beta}| = \frac{\sqrt{(c_{12}^2 c_{13}^2 m_1 + s_{12}^2 c_{13}^2 m_2 \cos \alpha + s_{13}^2 m_3 \cos \beta)^2 + (s_{12}^2 c_{13}^2 m_2 \sin \alpha + s_{13}^2 m_3 \sin \beta)^2}}{\quad} \quad (3)$$

The parameters involved are:

- the angles θ_{12} and θ_{13} , measured with good precision by the solar and short-baseline reactor neutrino experiments, respectively;
- the neutrino mass eigenstates m_1 , m_2 , and m_3 , which are related to the solar and atmospheric squared mass differences $\delta m_{\odot\oplus}^2$ and Δm_{atm}^2 :

$$\begin{aligned} \delta m_{\odot\oplus}^2 &\simeq \Delta m_{21}^2 \\ \Delta m_{\text{atm}}^2 &\simeq \frac{1}{2} |\Delta m_{31}^2 + \Delta m_{32}^2|. \end{aligned} \quad (4)$$

These are known with $\sim 3\%$ uncertainty thanks to long-baseline reactor and long-baseline accelerator neutrino experiments, respectively (see Table 1). The mass eigenstates are also related to the sum of neutrino masses,

$$\Sigma = \sum_{i=1}^3 m_i, \quad (5)$$

for which several upper limits of about 0.1–0.2 eV are set by cosmological observations [3–5];

- the two Majorana phases α and β , for which no experimental information is available.

The relation between the mass eigenstates and the squared mass differences given in Eq. 4 allows two possible orderings of the neutrino masses [6]. Using the same notation of [7],

Table 1 Parameters for the evaluation of the effective Majorana mass

Parameter	Value [2]
$\delta m_{\odot\oplus}^2$	$(7.54 \pm 0.26) \times 10^{-5} \text{ eV}^2$
Δm_{atm}^2 (NH)	$(2.43 \pm 0.06) \times 10^{-3} \text{ eV}^2$
Δm_{atm}^2 (IH)	$(2.38 \pm 0.06) \times 10^{-3} \text{ eV}^2$
s_{12}^2	$(3.08 \pm 0.17) \times 10^{-1}$
s_{13}^2 (NH)	$(2.34 \pm 0.20) \times 10^{-2}$
s_{13}^2 (IH)	$(2.40 \pm 0.22) \times 10^{-2}$
Σ	$(22 \pm 62) \times 10^{-3} \text{ eV}$ [4,5]

a first scheme, denoted the Normal Hierarchy (NH), corresponds to

$$\begin{aligned} m_1 &= m_{\min}, \\ m_2 &= \sqrt{m_{\min}^2 + \delta m_{\odot\oplus}^2}, \\ m_3 &= \sqrt{m_{\min}^2 + \Delta m_{\text{atm}}^2 + \frac{\delta m_{\odot\oplus}^2}{2}}, \end{aligned} \quad (6)$$

where m_{\min} is the mass of the lightest neutrino. The so-called Inverted Hierarchy (IH) is given by

$$\begin{aligned} m_1 &= \sqrt{m_{\min}^2 + \Delta m_{\text{atm}}^2 - \frac{\delta m_{\odot\oplus}^2}{2}}, \\ m_2 &= \sqrt{m_{\min}^2 + \Delta m_{\text{atm}}^2 + \frac{\delta m_{\odot\oplus}^2}{2}}, \\ m_3 &= m_{\min}. \end{aligned} \quad (7)$$

Present data do not show any clear preference for either of the two schemes.

3 Effective mass versus lightest neutrino mass

The effective mass can be expressed as a function of the lightest neutrino mass, as first introduced in [8]. This is normally done via a χ^2 analysis [7], where the uncertainties on the mixing angles θ_{12} and θ_{13} , and on the squared mass differences $\delta m_{\odot\oplus}^2$ and Δm_{atm}^2 are propagated, while the values of the Majorana phases leading to the largest and smallest $|m_{\beta\beta}|$ are considered. As a result, the 1σ , 2σ , and 3σ allowed regions are typically shown (e.g. Fig. 3 of [7]), but no clear information as regards the relative probability of different $|m_{\beta\beta}|$ values for a fixed m_{\min} is provided. This can become of dramatic importance in the case future experiments prove that nature chose the NH regime. In NH, the effective mass is distributed within a flat area between $\sim 10^{-3}$ and $\sim 5 \times 10^{-3}$ eV if $m_{\min} < 10^{-3}$ eV, while

it can vanish for $m_{\min} \in [10^{-3}, 10^{-2}]$ eV due to the combination of the Majorana phases. The case of a vanishing $|m_{\beta\beta}|$ is possible only for a smaller subset of values of the Majorana phases than the whole $[0, 2\pi]$ range. This does not necessarily mean that a vanishing effective mass implies that the theory suffers from dangerous fine tuning. Namely, in some models the effective mass can assume a naturally small value that remains small after renormalization due to the chiral symmetry of fermions [9, 10].

Without giving a preference to any model, one can ask which is the distribution probability of $|m_{\beta\beta}|$ for a fixed value of m_{\min} and, moreover, which is the probability for the NH case of having $|m_{\beta\beta}| < 10^{-3}$ eV given the present knowledge (or ignorance) of the various parameters involved. An answer is obtained using a toy Monte Carlo (MC) approach, where a random number is sampled for each parameter according to its (un)known measured value, and $|m_{\beta\beta}|$ is computed for each trial.

The values for the experimentally measured parameters are taken from Table 3 of [2]. In case the upper and lower error on some parameter are different, the random sampling is performed using a Gaussian distribution with mean given by the best fit of [2] and σ given by the greater among the upper and lower uncertainties. These values are reported in Table 1. The effect of this conservative choice on the resulting allowed regions for $|m_{\beta\beta}|$ vs m_{\min} is small, and the message of this study is not changed. Similarly, the use of a more recent and precise value for θ_{13} [11] does not significantly affect the result. An eventual correlation between the involved parameters could easily be included in the study. For the values of Table 1 it can be considered negligible and is not taken into account.

The choice not to prefer any model is reflected on the distribution assigned to the Majorana phases. Assuming a complete ignorance of α and β , their values are sampled from a flat distribution in the $[0, 2\pi]$ range.

A two dimensional histogram with increasing bin size is exploited. In particular, the bin width Δ_i is given by $\Delta_i = k\Delta_{i-1}$ with $k > 1$, for both the x and the y directions. This allows one to keep the bi-logarithmic scale normally used in the literature and at the same time to maintain the same normalization over all the considered area. For each bin of the x -axis, 10^6 random parameter combinations are used to calculate the probability distribution for $|m_{\beta\beta}|$, leading to the plot shown in Fig. 1. The different color levels correspond to the 1, 2, ..., 5 σ coverage regions. The sensitivity of the current experiments, at the 10^{-1} eV level, is reported, together with the sensitivity of an hypothetical ton scale experiment and the ultimate sensitivity of a 100 ton scale setup with the assumption of zero background.

Looking at the $|m_{\beta\beta}|$ population for both the IH and the NH, high values of $|m_{\beta\beta}|$ are favored for all values of m_{\min} . This can have a strong impact on the perspectives of $0\nu\beta\beta$

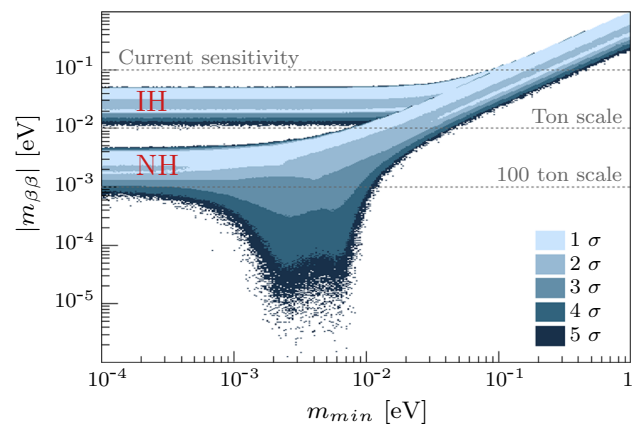


Fig. 1 Effective Majorana mass as a function of the lightest neutrino mass. The top band correspond to the IH regime, the bottom to NH. The different colors correspond to the 1, ..., 5 σ coverage regions

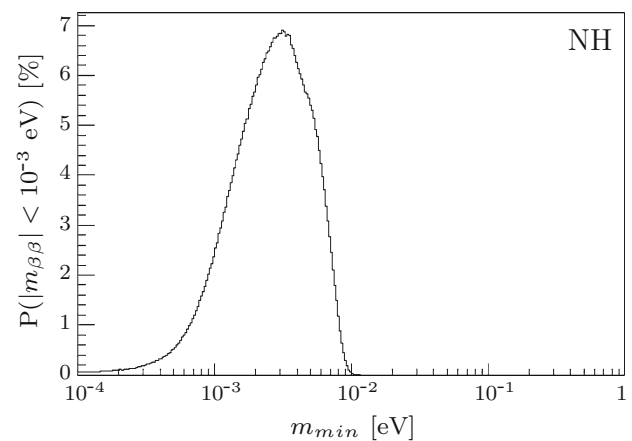


Fig. 2 Probability for $|m_{\beta\beta}| < 10^{-3}$ eV in the NH regime

decay search in the next decades. For the NH case, the probability of having $|m_{\beta\beta}| < 10^{-3}$ eV is reported in Fig. 2. Even for the most unfortunate case of $m_{\min} \sim 3\text{--}4 \times 10^{-3}$ eV, given the present knowledge of the oscillation parameters there is at least 93 % probability of detecting a $0\nu\beta\beta$ decay signal if an experiment with 10^{-3} eV discovery sensitivity on $|m_{\beta\beta}|$ is available. Such a sensitivity would involve the realization of an experiment with ~ 100 ton active mass operating in zero-background condition (see Sect. 5). If this is presently hard to imagine, some case studies have already been published on the topic [12]. On the other side, the creation of an experiment with 10^{-5} eV sensitivity would most probably be out of reach because it would involve the deployment of $\gtrsim 10^6$ ton of active material.

One can ask which values of the Majorana phases are needed in order to obtain $|m_{\beta\beta}| < 10^{-3}$ eV. This is shown in Fig. 3: small values of the effective mass are only possible if α and β differ by a value $\sim \pi$. With reference to Eq. 3, neglecting for the moment the term $c_{12}^2 c_{13}^2 m_1$ and supposing all other terms have the same amplitude, $|m_{\beta\beta}|$ approaches

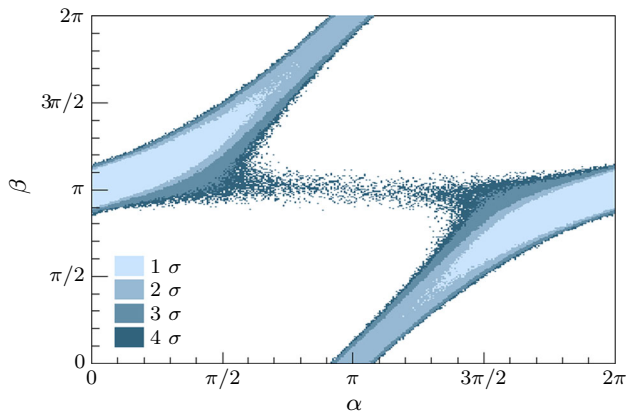


Fig. 3 Majorana phases α and β for $|m_{\beta\beta}| < 10^{-3}$ eV in the NH regime. The different colors correspond to the 1, ..., 4 σ coverage regions

zero only if both couples $(\sin \alpha, \sin \beta)$ and $(\cos \alpha, \cos \beta)$ have opposite signs. The condition is satisfied only if α and β belong to opposite quadrants. Considering the amplitude of the terms, the major difference is that $|m_{\beta\beta}|$ can become small for $m_{\min} \in [10^{-3}, 10^{-2}]$ eV and not for $m_{\min} = 0$, but the required correlation between the Majorana phases is unchanged. Hence, our result shows that in the type of models [9, 10] mentioned above the Majorana phases are closely correlated.

One remark has to be made regarding the sparsely populated region for $\alpha \in [\pi/2, 3\pi/2]$ and $\beta \sim \pi$ of Fig. 3. These points correspond to those in the region with $m_{\min} < 10^{-3}$ eV and $|m_{\beta\beta}| < 10^{-3}$ eV of Fig. 1, or in other words to the bottom left part of the horizontal NH band. Hence, they can be considered a spurious contamination coming from the choice of selecting the events with $m_{\min} < 10^{-3}$ eV.

4 How does cosmology affect $0\nu\beta\beta$ decay search?

In the analysis presented so far the effective mass depends on the three free parameters: the two Majorana phases are considered as nuisance parameters with uniform distribution, and the probability distribution for $|m_{\beta\beta}|$ as a function of m_{\min} is obtained.

Several cosmological measurements allow one to put upper bounds on the sum of neutrino masses, Σ . These limits are typically around 0.1–0.2 eV [3–5], depending on the considered data sets. Recently, a combined analysis of the Planck 2013 data and several Lyman- α forest data sets lead to a Gaussian probability distribution for Σ , with $\Sigma = (22 \pm 62) \times 10^{-3}$ eV [4, 5]. The corresponding 95 % CL limit is $\Sigma < 0.146$ eV. The distribution was already used in [5] to extract the allowed range for $|m_{\beta\beta}|$ as a function of Σ . In that case, the allowed regions for NH and IH are weighted with the cosmological bound on Σ , and it is pointed out that the allowed region for IH is strongly reduced.

The study can be extended including the cosmological bound following a different approach than that used in [5]. Considering Eqs. 5, 6 and 7, the three parameters m_1, m_2 , and m_3 depend on δm_{\odot}^2 , Δm_{atm}^2 , and Σ , for which a measurement is available. Hence, a random sampling is performed on δm_{\odot}^2 , Δm_{atm}^2 , and Σ , and the values of the mass eigenstates are extracted numerically after solving the system of Eqs. 5, 6 for NH, and 5, 7 for IH. Considering the NH case and given the measured values of the squared mass differences, Eq. 6 states that the minimum value of Σ is

$$\Sigma_{\min}^{\text{NH}} = \sqrt{\delta m_{\odot}^2} + \sqrt{\Delta m_{\text{atm}}^2 + \frac{\delta m_{\odot}^2}{2}} \simeq 0.058 \text{ eV} \quad (8)$$

where m_{\min} has been set to 0. Similarly, for IH:

$$\Sigma_{\min}^{\text{IH}} = \sqrt{\Delta m_{\text{atm}}^2 - \frac{\delta m_{\odot}^2}{2}} + \sqrt{\Delta m_{\text{atm}}^2 + \frac{\delta m_{\odot}^2}{2}} \simeq 0.098 \text{ eV}. \quad (9)$$

The combination of the cosmological bound with the measurements of δm_{\odot}^2 and Δm_{atm}^2 will therefore induce a probability distribution for Σ with a sharp rise at about 0.058(0.098) eV and a long high-energy tail for the NH(IH) regime.

The probability distributions for $|m_{\beta\beta}|$ as a function of Σ in the NH and IH cases are shown in Figs. 4 and 5, respectively. In total, 10^8 points are sampled. The thresholds on Σ correspond to the lower bounds mentioned above, while the horizontal shading for $\Sigma > 10^{-1}$ eV comes from the cosmological bound. In NH case, the vertical shading for $\Sigma \in [6, 7] \times 10^{-2}$ eV and $|m_{\beta\beta}| < 10^{-3}$ eV is related to the combination of the Majorana phases, as explained in Sect. 3.

It is worth mentioning that the approach used here does not allow one to make any statement regarding the overall probability of the NH with respect to the IH regime. The plots are populated by generating random numbers for δm_{\odot}^2 , Δm_{atm}^2 , and Σ according to the values reported in Table 1. If $\Sigma > \Sigma_{\min}$, with Σ_{\min} calculated for each sampled couples of δm_{\odot}^2 and Δm_{atm}^2 as given by Eqs. 8 and 9, the three values are accepted and $|m_{\beta\beta}|$ is computed. On the contrary, another random number is extracted for Σ until the condition is satisfied. In this way, Figs. 4 and 5 are equally populated, and they give no hint about the probability that nature chose either of the two regimes.

The plot of $|m_{\beta\beta}|$ as a function of m_{\min} with the application of the cosmological bound is shown in Fig. 6. Differently from Fig. 1, it not only provides the probability distribution for $|m_{\beta\beta}|$ as a function of m_{\min} , but also the 2-dimensional probability distribution for both parameters together. The main differences with respect to Fig. 1 are the decreases of the distribution for $m_{\min} \in [5 \times$

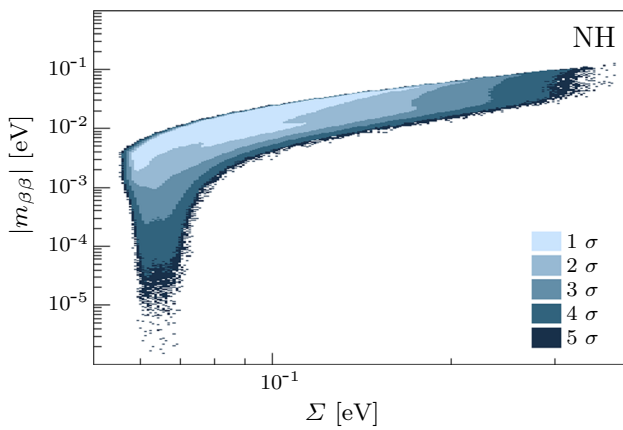


Fig. 4 Effective Majorana mass as a function of the sum of neutrino masses for the NH regime with the application of the cosmological bound. The different colors correspond to the 1, . . . , 5 σ coverage regions

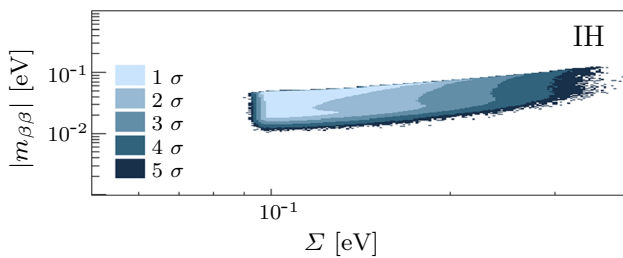


Fig. 5 Effective Majorana mass as a function of the sum of neutrino masses for the IH regime with the application of the cosmological bound. The different colors correspond to the 1, . . . , 5 σ coverage regions

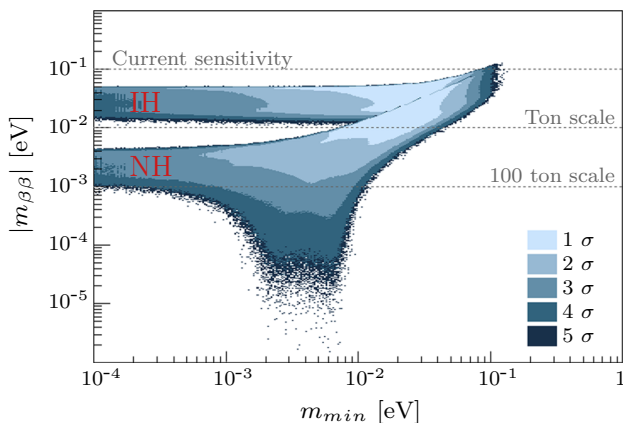


Fig. 6 Effective Majorana mass as a function of the lightest neutrino mass with the application of the cosmological bound. The different colors correspond to the 1, . . . , 5 σ coverage regions

$10^{-2}, 10^{-1}$] eV, and for $m_{\min} \lesssim 7 \times 10^{-3}$ eV. Both effects are due to the cosmological bound on Σ . Choosing arbitrarily different values for both the mean value and the width for the Gaussian distribution of the total neutrino mass leads to different shadings on both sides, and induces the

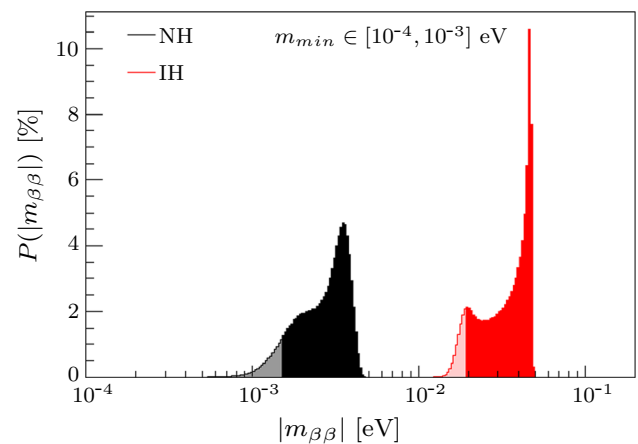


Fig. 7 Probability distribution for $|m_{\beta\beta}|$ with $m_{\min} \in [10^{-4}, 10^{-3}]$ eV. The darker regions correspond to the 90 % coverage on $|m_{\beta\beta}|$

highly populated region around $m_{\min} \sim 3 \times 10^{-2}$ eV to move. In particular, a looser bound on σ would favor the degenerate mass region, while a tighter limit would favor smaller values of m_{\min} , as expected, with strong consequences for the predicted $|m_{\beta\beta}|$. With the present assumptions, values of $|m_{\beta\beta}|$ close to the degenerate region are favored.

With an eye on the future experiments, the probability distribution for $|m_{\beta\beta}|$ only can be obtained by marginalizing the 2-dimensional distribution of Fig. 6 over m_{\min} . This is performed separately for three ranges of the lightest neutrino mass: $m_{\min} \in [10^{-4}, 10^{-3}]$ eV, $m_{\min} \in [10^{-3}, 10^{-2}]$ eV and $m_{\min} \in [10^{-2}, 10^{-1}]$ eV as shown in Figs. 7, 8 and 9. In case of a small m_{\min} (Fig. 7) the 90 % coverage is obtained for $|m_{\beta\beta}| > 1.54 \times 10^{-3}$ eV and $|m_{\beta\beta}| > 1.96 \times 10^{-2}$ eV for NH and IH, respectively. In general, for IH high values of $|m_{\beta\beta}|$ are favored. The 90 % coverage on $|m_{\beta\beta}|$ for the three considered ranges are reported in Table 2, together with that of the overall range $m_{\min} \in [10^{-4}, 1]$ eV. This case shows how a 3.32×10^{-3} eV discovery sensitivity is required for future experiments in order to have 90 % probability to measure a $0\nu\beta\beta$ decay signal in the case of NH, or 2.14×10^{-2} eV for IH.

The strong dependence of the result both on the choice of the Majorana phases distribution and on the cosmological bound should invoke some caution in the interpretation of Figs. 6, 7, 8, and 9 as the correct probability distributions for $|m_{\beta\beta}|$. It is rather important to enlighten the fact that it is in principle possible, making some arbitrary assumption on the Majorana phases and provided a reliable cosmological limit on the total neutrino mass, to extract a probability distribution for $|m_{\beta\beta}|$. A higher precision of the cosmological measurement, e.g. by EUCLID [13, 14], would strongly improve the reliability of a prediction on $|m_{\beta\beta}|$.

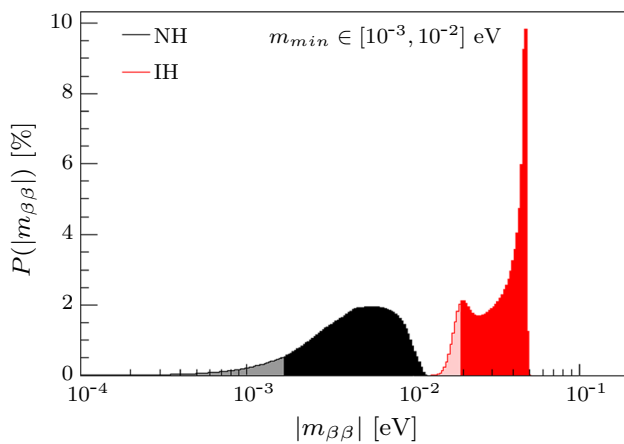


Fig. 8 Probability distribution for $|m_{\beta\beta}|$ with $m_{\min} \in [10^{-3}, 10^{-2}]$ eV. The darker regions correspond to the 90 % coverage on $|m_{\beta\beta}|$

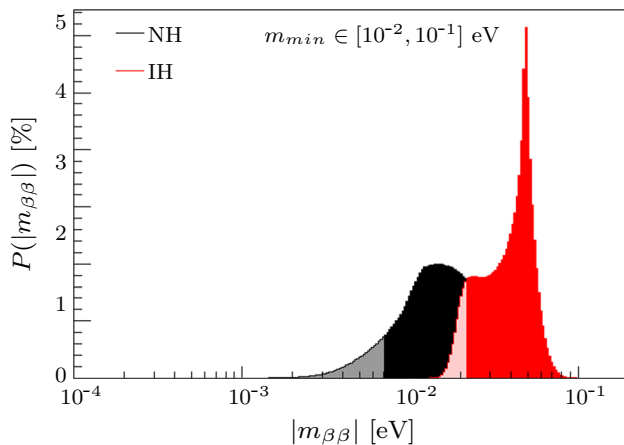


Fig. 9 Probability distribution for $|m_{\beta\beta}|$ with $m_{\min} \in [10^{-2}, 10^{-1}]$ eV. The darker regions correspond to the 90 % coverage on $|m_{\beta\beta}|$

Table 2 90 % coverage on $|m_{\beta\beta}|$ for NH and IH and different ranges of m_{\min}

m_{\min} [eV]	$ m_{\beta\beta} $ 90 % coverage [eV]	
	NH	IH
$[10^{-4}, 10^{-3}]$	$>1.54 \times 10^{-3}$	$>1.96 \times 10^{-2}$
$[10^{-3}, 10^{-2}]$	$>1.68 \times 10^{-3}$	$>1.96 \times 10^{-2}$
$[10^{-2}, 10^{-1}]$	$>7.16 \times 10^{-3}$	$>2.20 \times 10^{-2}$
$[10^{-4}, 1]$	$>3.32 \times 10^{-3}$	$>2.14 \times 10^{-2}$

5 From effective mass to $0\nu\beta\beta$ decay half life

From an experimental point of view, it is useful to compute the probability distribution for the $0\nu\beta\beta$ decay half life ($T_{1/2}^{0\nu}$) as a function of the lightest neutrino mass. The relation between $T_{1/2}^{0\nu}$ and the effective mass is [1]:

$$\frac{1}{T_{1/2}^{0\nu}} = G^{0\nu} g_A^4 |\mathcal{M}^{0\nu}|^2 \frac{|m_{\beta\beta}|^2}{m_e^2} \quad (10)$$

where $G^{0\nu}$ is the phase space integral, g_A the axial vector coupling constant, $|\mathcal{M}^{0\nu}|$ the nuclear matrix element (NME), and m_e the electron mass. Considering different $\beta\beta$ decaying isotopes and for a fixed effective mass, greater values of the phase space integral and NME correspond to a shorter $0\nu\beta\beta$ decay half life and, consequently, to a greater specific activity.

If a higher $Q_{\beta\beta}$ would in principle allow for a higher phase space integral, the Coulomb potential of the daughter nucleus plays a strong role in the calculation [15]. The value of $G^{0\nu}$ is around 10^{-15} – 10^{-14} year $^{-1}$, depending on the isotope.

The calculation of $|\mathcal{M}^{0\nu}|$ is usually the bottleneck for the extraction of $|m_{\beta\beta}|$ from Eq. 10. Even though a strong effort is being made in working on the problem, different nuclear models yield $|\mathcal{M}^{0\nu}|$ values which can vary by more than a factor two. A compilation of possible estimations for the most investigated $\beta\beta$ emitting isotopes is given in [16].

The estimation of g_A is still matter of debate [17, 18]. Namely it is not clear if the value for free nucleons has to be considered, or if some “quenching” is induced by limitations in the calculation or by the omission of non-nucleonic degrees of freedom. Given this ambiguity, the effect of the quenching of g_A is not considered here, and only unquenched values are used.

Among the dozen $\beta\beta$ decaying isotopes, ^{76}Ge , ^{130}Te and ^{136}Xe are of particular interest due to the existence of established technologies that led to the construction in the past years of several experiments which set limits of ~ 0.2 to 0.5 eV on $|m_{\beta\beta}|$ [19–22]. The next phase experiments employing these isotopes will allow one to start probing or partially cover the IH region, depending on the case.

From an experimental perspective, it is important to estimate the required sensitivity on $T_{1/2}^{0\nu}$ in order to cover the IH or the NH region using ^{76}Ge , ^{130}Te and ^{136}Xe . The probability distributions for $T_{1/2}^{0\nu}$ as a function of m_{\min} with the application of the cosmological bound for the three isotopes are shown in Figs. 10, 11 and 12 for NH (top) and IH (bottom). The contour lines correspond to the 1–5 σ coverage regions. The distributions have been extracted from that of $|m_{\beta\beta}|$ with the application of Eq. 10. The values for the phase space integral are taken from [15], and the NME from [16], and reported in Table 3. Given the large span between different NME estimations, the largest and the smallest NME reported in [16] are used. These correspond to the blue and red distributions in Figs. 10, 11, and 12, respectively. For ^{76}Ge , the IH band for the optimal NME starts at $6\text{--}7 \times 10^{27}$ year, while for ^{130}Te and ^{136}Xe it starts at 2×10^{26} year and 3×10^{26} year, respectively. In this regard, ^{130}Te and ^{136}Xe are preferable with respect to ^{76}Ge . In reality, the total efficiency, the energy resolution, the atomic mass and the isotopic fraction of the

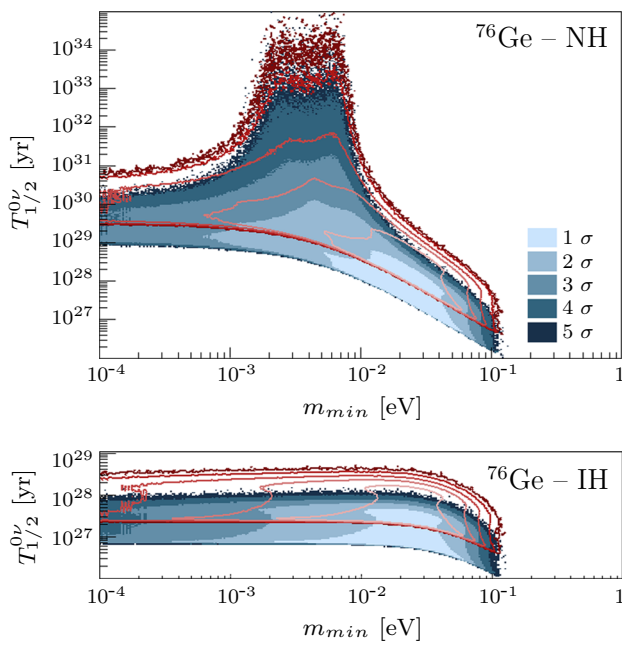


Fig. 10 $0\nu\beta\beta$ decay half life for ^{76}Ge as a function of the lightest neutrino mass with the application of the cosmological bound. The blue regions are obtained with $|\mathcal{M}^{0\nu}| = 5.16$, the red curves with $|\mathcal{M}^{0\nu}| = 2.81$. The different color shadings correspond to the 1, . . . , 5 σ coverage regions

considered isotopes have to be considered, too. A complete review of the topic is given in [23, 24].

If IH is assumed and considering the smallest NME, an experiment aiming to measure $0\nu\beta\beta$ decay needs a sensitivity on $T_{1/2}^{0\nu}$ of $\sim 4 \times 10^{28}$ year if ^{76}Ge is employed, or of $\sim 9 \times 10^{27}$ year with ^{130}Te and ^{136}Xe . Assuming NH and an effective mass of 10^{-3} eV, a ^{76}Ge -based experiment would need a sensitivity of $\sim 6 \times 10^{30}$ year, while with ^{130}Te and ^{136}Xe a $\sim 10^{30}$ year sensitivity is sufficient.

One remark can be made with respect to the debated Klapdor-Kleingrothaus claim of $0\nu\beta\beta$ decay observation in ^{76}Ge [25]. In Fig. 10 the 5 σ coverage region for the largest NME (blue curves) does not extend below 10^{26} year. This is in very strong tension with the published 99.73 % CL interval for the $0\nu\beta\beta$ decay half life, $T_{1/2}^{0\nu} = (0.69 - 4.18) \times 10^{25}$ year [25]. In other words, assuming that only the standard three light neutrino participate to $0\nu\beta\beta$ decay and using the largest NME and an unquenched g_A , a $> 5 \sigma$ disagreement is present between the cosmological bound and the Klapdor-Kleingrothaus claim.

6 Perspectives for electron neutrino mass measurements

A side product of the present study is the behavior of $|m_{\beta\beta}|$ as a function of the electron neutrino mass, m_β . This is the parameter of interest for the experiments measur-

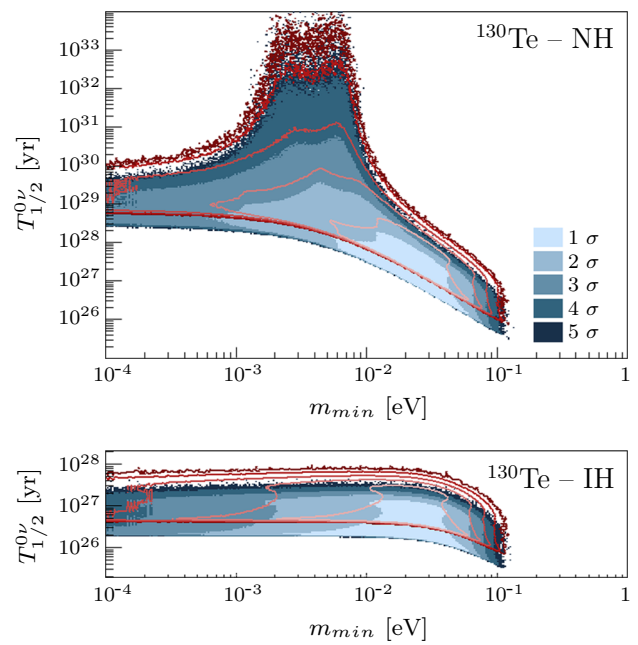


Fig. 11 $0\nu\beta\beta$ decay half life for ^{130}Te as a function of the lightest neutrino mass with the application of the cosmological bound. The blue regions are obtained with $|\mathcal{M}^{0\nu}| = 3.89$, the red curves with $|\mathcal{M}^{0\nu}| = 2.65$. The different color shadings correspond to the 1, . . . , 5 σ coverage regions

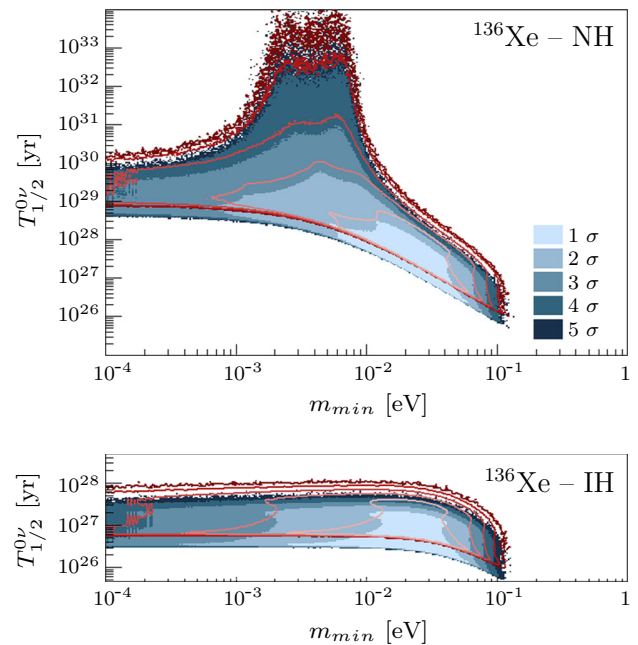


Fig. 12 $0\nu\beta\beta$ decay half life for ^{136}Xe as a function of the lightest neutrino mass with the application of the cosmological bound. The blue regions are obtained with $|\mathcal{M}^{0\nu}| = 3.05$, the red curves with $|\mathcal{M}^{0\nu}| = 2.18$. The different color shadings correspond to the 1, . . . , 5 σ coverage regions

ing the end point of beta spectra, e.g. KATRIN [26] and Project8 [27], or the ^{163}Ho electron capture, e.g. ECHO [28] and HOLMES [29]. The electron neutrino mass is given by

Table 3 $0\nu\beta\beta$ decay phase space factors, together with the smallest and largest NME for ^{76}Ge , ^{130}Te and ^{136}Xe . The values of $G^{0\nu}$ are taken from [15], the NME from [16]. For each NME, the nuclear model used for the calculation is reported. The value of g_A considered for ISM is 1.25, for QRPA-Tü $g_A = 1.27$, and for IBM-2 $g_A = 1.269$

Isotope	$G^{0\nu} [10^{-15} \text{year}^{-1}]$	$ \mathcal{M}^{0\nu} $	
		Smallest	Largest
^{76}Ge	2.363	2.81 (ISM)	5.16 (QRPA-Tü)
^{130}Te	14.22	2.65 (ISM)	3.89 (QRPA-Tü)
^{136}Xe	14.58	2.18 (QRPA-Tü)	3.05 (IBM-2)

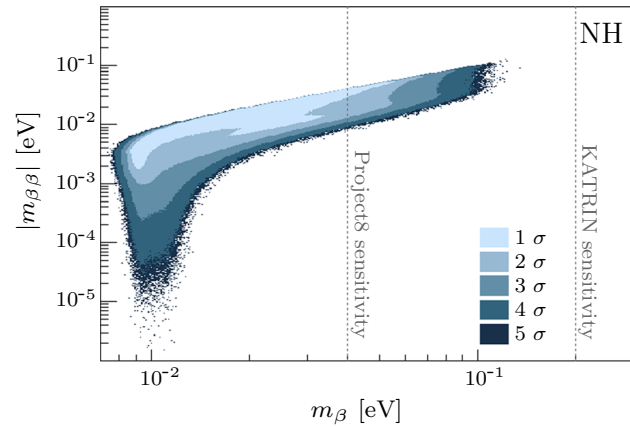


Fig. 13 Effective Majorana mass as a function of the electron neutrino mass for the NH regime with the application of the cosmological bound. The different color shadings correspond to the 1, . . . , 5 σ coverage regions

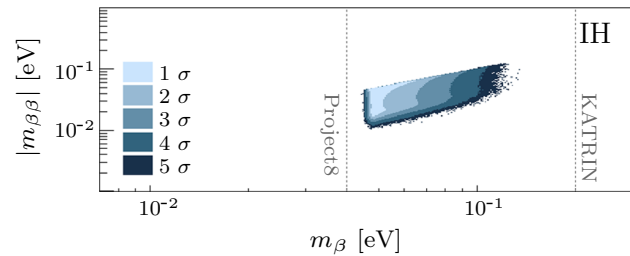


Fig. 14 Effective Majorana mass as a function of the electron neutrino mass for the IH regime with the application of the cosmological bound. The different color shadings correspond to the 1, . . . , 5 σ coverage regions

$$\begin{aligned}
 m_{\beta} &= \sqrt{\sum_{i=1}^3 |U_{ei}|^2 m_i^2} \\
 &= \sqrt{c_{13}^2 c_{12}^2 m_1^2 + c_{13}^2 s_{12}^2 m_2^2 + s_{13}^2 m_3^2}, \tag{11}
 \end{aligned}$$

where no new physics is involved with respect to the standard model. Figures 13 and 14 show $|m_{\beta\beta}|$ as a function of m_{β} for the NH and IH, respectively. The minimum of m_{β} comes from the values of δm_{\odot}^2 and Δm_{atm}^2 , while the shading for

$m_{\beta} \gtrsim 5 \times 10^{-2}$ eV is governed by the cosmological limit on Σ . The vertical dashed lines correspond to the sensitivity of KATRIN at 0.2 eV [26,30], and of the recently proposed Project8 experiment at 40 meV [27]. It is interesting to see how strongly the cosmological observations affect the expectation for m_{β} . Assuming $\Sigma = (22 \pm 62) \times 10^{-3}$ eV [4,5], the probability for KATRIN to find a signal is practically zero. Even using an arbitrarily looser bound on Σ , the chance for m_{β} to be at the 0.2 eV level remains very limited. On the contrary, the cosmological bound does not really affect the physics reach of Project8. Its goal sensitivity is sufficient to fully cover the IH region: if nature chose IH, the cosmological bound cannot exclude all values of m_{β} down to 40 meV without being in conflict with the measurements of δm_{\odot}^2 and Δm_{atm}^2 . If the target sensitivity is reached, Project8 would have very good chances of discovery. If neutrino masses follow the NH scheme, the allowed range for m_{β} would extend down to ~ 8 meV. At present, no technology is capable of reaching such a sensitivity, and the possibility to measure the electron neutrino mass might be unreachable.

7 Conclusions

In this work, a new method for the calculation of the allowed range for $|m_{\beta\beta}|$ and $T_{1/2}^{0\nu}$ in the standard three neutrino scheme is proposed. It is based on the random sampling of the involved mixing angles, of the squared neutrino masses and of the Majorana phases. The effect of these on $|m_{\beta\beta}|$ is highlighted, and the consequences for $0\nu\beta\beta$ decay search are described. The assumption of a flat distribution in the $[0, 2\pi]$ region for the Majorana phases yields a $\geq 93\%$ discovery probability for an experiment with 10^{-3} eV sensitivity on $|m_{\beta\beta}|$. Smaller $|m_{\beta\beta}|$ values can be obtained only if the Majorana phases differ by $\sim \pi$. Based on this, theoretical models for the neutrino mass matrix predicting a small $|m_{\beta\beta}|$ [9,10] are expected to have Majorana phases which obey this condition.

In a second step, the cosmological bound on Σ is applied, leading to the two dimensional probability distribution for $|m_{\beta\beta}|$ as a function of the lightest neutrino mass. A weak preference for $|m_{\beta\beta}|$ values close to the degenerate region is found, although the strong dependence on the probability distribution for Σ invokes some caution in the extraction of predictions. A 3.3×10^{-3} eV discovery sensitivity on $|m_{\beta\beta}|$ in the case of NH and 2.1×10^{-2} eV in the case of IH are required to future experiments in order to achieve a 90% probability of measuring $0\nu\beta\beta$ decay.

Moreover, the probability distribution for the $0\nu\beta\beta$ decay half life as a function of the lightest neutrino mass for ^{76}Ge , ^{130}Te and ^{136}Xe is given. This shows how a sensitivity of $O(10^{28})$ year on $T_{1/2}^{0\nu}$ is required for all three isotopes to cover the IH region, while in the case of NH a sensitivity of $O(10^{30})$ year is needed.

Finally, the perspectives for the direct measurement of the electron neutrino mass with β -decay end point experiments are discussed, and the possibility of discovery for an experiment with 40 meV sensitivity is shown, under the assumption that neutrino masses are distributed according to the IH.

Acknowledgments The author gratefully thanks L. Baudis, R. Brugnera, G. Isidori, L. Pandola, B. Schwingenheuer and F. Vissani for the enlightening suggestions, and P. Grabmayr and B. Schwingenheuer for carefully checking the manuscript.

Open Access This article is distributed under the terms of the Creative Commons Attribution 4.0 International License (<http://creativecommons.org/licenses/by/4.0/>), which permits unrestricted use, distribution, and reproduction in any medium, provided you give appropriate credit to the original author(s) and the source, provide a link to the Creative Commons license, and indicate if changes were made. Funded by SCOAP³.

References

1. S.M. Bilenky, C. Giunti, *Int. J. Mod. Phys. A* **30**, 1530001 (2015). [arXiv:1411.4791](#)
2. F. Capozzi et al., *Phys. Rev. D* **89**, 093018 (2014). [arXiv:1312.2878](#)
3. Planck, P.A.R. Ade et al., (2015). [arXiv:1502.01589](#)
4. N. Palanque-Delabrouille et al., *JCAP* **1502**, 045 (2015). [arXiv:1410.7244](#)
5. S. Dell’Oro, S. Marcocci, M. Viel, F. Vissani, (2015). [arXiv:1505.02722](#)
6. Particle Data Group, K.A. Olive et al., *Chin. Phys. C* **38**, 090001 (2014)
7. C. Giunti, E.M. Zavanin, *JHEP* **07**, 171 (2015). [arXiv:1505.00978](#)
8. F. Vissani, *JHEP* **06**, 022 (1999). [arXiv:hep-ph/9906525](#)
9. F. Vissani, M. Narayan, V. Berezinsky, *Phys. Lett. B* **571**, 209 (2003). [arXiv:hep-ph/0305233](#)
10. F. Vissani, *Phys. Lett. B* **508**, 79 (2001). [arXiv:hep-ph/0102236](#)
11. Daya Bay, F.P. An et al., *Phys. Rev. Lett.* **115**, 111802 (2015). [arXiv:1505.03456](#)
12. S.D. Biller, *Phys. Rev. D* **87**, 071301 (2013). [arXiv:1306.5654](#)
13. EUCLID, R. Laureijs et al., (2011). [arXiv:1110.3193](#)
14. J. Hamann, S. Hannestad, Y.Y.Y. Wong, *JCAP* **1211**, 052 (2012). [arXiv:1209.1043](#)
15. J. Kotila, F. Iachello, *Phys. Rev. C* **85**, 034316 (2012). [arXiv:1209.5722](#)
16. J. Barea, J. Kotila, F. Iachello, *Phys. Rev. C* **91**, 034304 (2015). [arXiv:1506.08530](#)
17. J. Barea, J. Kotila, F. Iachello, *Phys. Rev. C* **87**, 014315 (2013). [arXiv:1301.4203](#)
18. R.G.H. Robertson, *Mod. Phys. Lett. A* **28**, 1350021 (2013). [arXiv:1301.1323](#)
19. GERDA Collaboration, M. Agostini et al., *Phys. Rev. Lett.* **111**, 122503 (2013). [arXiv:1307.4720](#)
20. CUORE, K. Alfonso et al., *Phys. Rev. Lett.* **115**, 102502 (2015). [arXiv:1504.02454](#)
21. EXO-200, J.B. Albert et al., *Nature* **510**, 229 (2014). [arXiv:1402.6956](#)
22. KamLAND-Zen, A. Gando et al., *Phys.Rev.Lett.* **110**, 062502 (2013). [arXiv:1211.3863](#)
23. J.J. Gomez-Cadenas, J. Martin-Albo, M. Mezzetto, F. Monrabal, M. Sorel, *Riv. Nuovo Cim.* **35**, 29 (2012). [arXiv:1109.5515](#)
24. B. Schwingenheuer, *Ann. Phys.* **525**, 269 (2013). [arXiv:1210.7432](#)
25. H.V. Klapdor-Kleingrothaus, I.V. Krivosheina, A. Dietz, O. Chkvorets, *Phys. Lett. B* **586**, 198 (2004). [arXiv:hep-ph/0404088](#)
26. KATRIN, A. Osipowicz et al., (2001). [arXiv:hep-ex/0109033](#)
27. Project 8, P.J. Doe et al., (2013). [arXiv:1309.7093](#)
28. L. Gastaldo et al., *J. Low Temp. Phys.* **176**, 876 (2014). [arXiv:1309.5214](#)
29. B. Alpert et al., *Eur. Phys. J. C* **75**, 112 (2015). [arXiv:1412.5060](#)
30. G. Drexlin, *Eur. Phys. J. C* **33**, S808 (2004)